J Appl Electrochem (2013) 43:559–565
DOI 10.1007/s10800-013-0548-z

ORIGINAL PAPER

Electrochemical performance of ionic liquid-molybdenum disulfide Li-ion batteries

D. Albrecht · H. Wulfmeier · S. Ivanov · A. Bund · H. Fritze

Received: 19 December 2012 / Accepted: 4 April 2013 / Published online: 17 April 2013

Abstract In this work, molybdenum disulfide (MoS_2) nanostructures with three different morphologies are synthesized and tested with respect to their applicability as anode material in lithium ion batteries with ionic liquid-based electrolytes. The nanostructured samples are compared with thin-film samples to evaluate the influence of the morphologies on the electrochemical performance. Characterization methods include X-ray diffraction, cyclic voltammetry, galvanostatic cycling, and thin-film calorimetry. The thin-film samples show a reversible capacity of 525 mAh g^{-1}, whereas for the nanostructured samples a maximum capacity 225 mAh g^{-1} is found.

Keywords Lithium ion battery · Nanostructures · Anode · Ionic liquid · Molybdenum disulfide · Thin-film calorimetry

1 Introduction

Environmental concerns as well as the continuously increasing use of renewable energy stimulate research efforts toward improved energy storage systems. For example, the technological change from fossil fuel to electrically driven vehicles requires high volumetric storage capacity as, in principle, provided by lithium ion batteries. However, the electric vehicles available on the market today suffer from poor battery lifetime as well as a lack of cruising range compared to established combustion engines.

One approach to improve the properties of secondary storage systems is the use of specially designed nanocrystalline morphologies for the electrode materials to increase the specific surface area, compensate the internal stress during intercalation and to shorten the diffusion length of the ions. Further, many commercially available lithium ion batteries are based on the graphite/polymer/$LiCoO_2$ system. While the cyclability of this system is satisfying (800–1,000 cycles), the volumetric as well as gravimetric capacities are insufficient. Another drawback of this system is the insufficient ionic conductivity of the polymer electrolytes, which is several magnitudes lower than that of the $LiPF_6$–organic carbonate solutions used for liquid electrolytes [1]. Despite their low conductivity, these polymer-based electrolytes are used because of their improved safety features. Therefore, the research objective should include the enhancement of the electrolyte conductivity without compromises on the safety issues as well as an increase in capacity without loosing cycling stability. We are trying to realize both aims in this study.

This work focuses on MoS_2 as an anode material for lithium ion batteries and the preparation of nanocrystalline and amorphous morphologies. MoS_2 recently attracted strong research efforts to replace common carbon anodes in lithium ion batteries [2–6]. MoS_2 microparticles show several advantages compared to the standard anode material graphite, which has a maximum capacity of 372 mAh g^{-1}. Key features are the high specific capacity (1st cycle: >1,000 mAh g^{-1}, 20th cycle: 800 mAh g^{-1} [7]) accompanied by a comparably low volume expansion (6.4 % for changes from $x = 0$ to 0.75 in Li_xMoS_2 [8]) as well as

D. Albrecht (✉) · H. Wulfmeier · H. Fritze
Institute of Energy Research and Physical Technologies, Clausthal University of Technology, Am Stollen 19B, 38640 Goslar, Germany
e-mail: daniel.albrecht@efzn.de

S. Ivanov · A. Bund
Department of Electrochemistry and Electroplating, Ilmenau University of Technology, Gustav Kirchhoff Straße 6, 98693 Ilmenau, Germany

improved breakdown features since the small cavities in between the nanotubes act as diffusion barriers for water [9]. Furthermore, the high operating voltage (>1 V) suppresses the formation of the solid electrolyte interface (SEI), which is one of the main sources of irreversible capacities and increased internal cell resistance. Decreasing the thickness of the SEI is expected to improve the cell performance. In addition, MoS_2 is cheap, non-toxic, widely available and shows a great variety of morphologies. Since MoS_2 is able to reversibly intercalate lithium ions in the amorphous state, thin-films and their applicability in lithium ion batteries are of interest as well. Several investigations show that amorphous MoS_2 performs properly in lithium ion batteries [10]. Compared to crystalline samples, they feature a higher diffusion coefficient, higher conductivity as well as a higher capacity combined with better cycling stability. Solid-state thin-film batteries have a wide range of potential applications in e.g., medical devices, mobile consumer electronics, or microsensor applications. The possibility to produce extremely thin batteries, especially tailored to the device of interest can be very useful. For medical applications like hearing aid, the miniaturization of the batteries is a key aspect. In mobile consumer electronics (mobiles, notebooks, tablets, etc.), the battery very often is the biggest component. Thin-film batteries open up the possibility to tailor the size and shape of a battery.

Another focus in this work is the interaction of the lithium ion containing ionic liquid (IL) (1M Li^+TFSI^-, [BMP][TFSI]) as electrolyte in a lithium ion cell with a MoS_2 anode. The use of the IL instead of the conventional ethylene carbonate, dimethyl carbonate (EC:DMC)-based electrolytes opens the possibility to work in a wider potential window [11]. This enables the use of MoS_2 in a high voltage cell if used with a 5 V cathode material like $LiCr_{0.2}Ni_{0.4}Mn_{1.4}O_4$ [12]. Safety is another motivation to apply wide range stable ILs since the commonly used alkyl carbonate-based electrolytes can be electrochemically oxidized even below 4 V versus Li/Li^+ [13]. ILs are, in contrast, electrochemically stable as well as inflammable. So, the use of IL-based electrolytes delivers enhanced conductivity compared to polymer electrolytes, improved cell safety and the option to increase the cell voltage (and therewith the energy density) using high voltage cathodes. To the best of our knowledge, the combination of MoS_2 as an anode material in a lithium ion battery based on an ionic liquid electrolyte has not been investigated before.

2 Experiment

2.1 Synthesis of molybdenum disulfide nanostructures

Nanocrystalline MoS_2 samples were synthesized via different hydrothermal routes in acidic media. Compared to other synthesis and preparation routes, this approach provides several advantages since it does not require the assistance of a template, high-temperature treatments ($T > 300$ °C like in CVD processes), or the use of gaseous H_2S (except for one route).

For the first route, in the following referred to as Route (1), ammonium heptamolybdate tetrahydrate [$(NH_4)_6Mo_7O_{24}\cdot 4H_2O$], sulfocarbamide ($CS(NH_2)_2$) and oxalic acid ($H_2C_2O_4\cdot 2H_2O$) were used as precursors. These analytically pure powders were weighed (2.47 g of $(NH_4)_6Mo_7O_{24}$, 2.12 g of $CS(NH_2)_2$ and 1.76 g of $H_2C_2O_4$), mortared and mixed with a few drops of water to form a highly viscous mixture. This mixture was put in a 30 ml Teflon-lined autoclave, sealed and heat treated at 220 °C for 24 h. Afterward, the as prepared solid was calcinated in a tube furnace at 620 °C for 2 h in nominally pure argon. The process follows largely the synthesis described in [7].

Route (2) was initially presented in [14]. In this approach, ammonium heptamolybdate tetrahydrate ($(NH_4)_6Mo_7O_{24}\cdot 4H_2O$), citric acid monohydrate ($C_6H_8O_7\cdot H_2O$) and sodium sulfur (Na_2S) were used as precursors. First, 0.98 g of ammonium heptamolybdate was put in 20 ml distilled water and mixed with a magnetic stirrer. After several minutes, 0.4 g citric acid and 0.25 g sodium sulfide crystals were added. This solution was put in a 30 ml Teflon-lined autoclave, sealed and heat treated for 24 h at 180 °C. The MoS_2 powder was separated from the solution via centrifugation, washed with ethanol and vacuum dried.

Route (3) is a variation of another route presented in [14]. As precursors ammonium heptamolybdate tetrahydrate ($(NH_4)_6Mo_7O_{24}\cdot 4H_2O$), hydrogen sulfur ($H_2S$) and hydrochloric acid (HCl) were used. First, 0.5 g ammonium heptamolybdate tetrahydrate were mixed into 25 ml distilled water using a magnetic stirrer. Afterward, this solution was acidified with dilute hydrochloric acid to a pH value slightly below 1 and warmed to 40 °C. Through this solution, H_2S gas was passed for about 7 min. The resulting solution was sealed in a 30 ml Teflon-lined autoclave and heat treated for 24 h at 180 °C.

2.2 Preparation of thin-films

MoS_2 thin-films were prepared by pulsed laser deposition (PLD) using a KrF excimer laser (COMPex 205, Lambda Physics) with pulse energies of 150–250 mJ and a pulse length of 25 ns. In order to prepare targets, the as prepared powders were cold pressed at 35 MPa with subsequent heat treatment at 600 °C for several hours in nominally pure argon. The film deposition was carried out in UHV ($p < 10^{-5}$ mbar). For the electrochemical characterization, a 250 nm thin-film was prepared on a 25 μm copper foil substrate.

2.3 Characterization methods

X-ray diffraction patterns of the nanostructures were recorded with a diffractometer (D5000, Siemens AG) using monochromatized Cu Kα radiation. Structural analysis was realized using a SEM (EcoMA 10, Carl Zeiss AG). For galvanostatic and potentiostatic characterization, a potentiostat/galvanostat (VMP3, BioLogic) in a three-electrode configuration was used. The determination of the specific surface area was done using the BET method (Gemini 2360, Micromeritics).

Beside those standard methods, thin-film calorimetry (TFC) was performed using high-temperature stable piezoelectric resonators. Those bulk acoustic wave resonators (langasite, $La_3Ga_5SiO_{14}$, Siccas, China) serve as highly sensitive temperature sensors by monitoring their temperature-dependent resonance frequency as described in [15]. For electrical characterization, the resonators have to be contacted with keyhole-shaped electrodes from both sides. Here, a combination of Ti and Pt/Rh deposited via PLD was used. These electrodes are chemically and thermally stable even in harsh environments [16]. Afterward, the material of interest was applied by a method of choice. For the experiments described here, the active material was deposited by PLD. The UHV chamber used for battery materials is portable, so it can be transferred into a glove box for sample handling. After deposition, the coated resonator was contacted with Pt-wires and installed in a gas tight quartz glass tube. This tube was installed in a furnace and purged with argon. The furnace was heated at constant rate of 1 K min^{-1}. For calorimetric measurements, the resonance frequency was tracked using an Agilent network analyzer and self made data processing software.

2.4 Li-ion cell preparation

In order to prepare electrodes the as prepared powders were mixed with 20 % carbon black and 10 % PVDF solved in NMP before being deposited as a 160 μm film on Cu foil. The drying process was carried out in two steps. First, the as prepared electrodes were heated in a furnace at 80 °C for several hours to reduce the amount of solvent. To further reduce the amount of water, the electrodes were heated above 150 °C under vacuum in combination with a nitrogen trap. Lithium ion cells were assembled in a self made PTFE cell setup in dry argon atmosphere with <1 ppm of water and oxygen in a glove box. For the determination of the long term cycling stability, coin cells with metallic lithium counter electrodes and polyethen separators (MTI Corporation, USA) were used. 1M Li^+TFSI^-, [BMP][TFSI] was applied as electrolyte and metallic lithium as counter and reference electrode. BMP and TFSI were purchased from IoLiTech. All the other chemicals described here were purchased from Alfa Aesar.

3 Results and discussion

SEM images of the nanostructures reveal significant differences in morphologies depending on the applied synthesis route and several process parameters like temperature, hydrothermal treatment duration, precursor concentration as well as postsynthesis treatment. Samples prepared via Route (1) exhibit a very porous, flower-like structure with large specific surface area (see Fig. 1a). Particle size ranges from 2 to 10 μm. A fine substructure and a porous surface are found. The specific surface area of these samples is determined by BET and found to be between 0.8 and 1.3 m^2 g^{-1}. The CV shows three peaks at 2.4, 1.9 and 1.6 V on the oxidizing path and a superposition of peaks at 1.60 V on the reducing path (Fig. 2a). In the initial cycle, there is an additional peak at 0.4 V, which can be attributed to the SEI formation [5].

Bundles of nanotubes with a predominant direction of growth are prepared via Route (2) (Fig. 1b). The properties of the tubular samples such as length and diameter can be tuned via the synthesis parameters. BET analysis delivered a specific surface area of 9.1–10.1 m^2 g^{-1}. Cyclic voltammetry performed on this sample shows two peak couples at 1.65 and 2.05 V on the oxidizing and 1.45 and 1.25 V on the reducing path (Fig. 2b).

The samples produced using Route (3) show large nanoflake agglomerates of 0.2–0.8 μm in size (Fig. 1c). Since the agglomerates of particles are very porous, the specific surface area is sufficiently large for lithium ion battery applications, even though the samples show no visible substructure. In comparison with the other powders these samples exhibit the largest specific surface area with 93.3–178.5 m^2 g^{-1}. CV shows two peak couples at 1.70 and 2.15 V on the oxidizing and 1.40 and 1.05 V on the reducing path (Fig. 2c).

SEM images of the thin-film sample exhibit a closed film with a large number of droplets (Fig. 1d). Here, cyclic voltammetry shows very broad peaks. This can be attributed to the amorphous state of PLD films [17] as well as to the small amount of active material. The centers of these broad peaks can be approximated to 1.15, 1.55, 1.87, and 2.35 V on the oxidizing path and 2.05, 1.18, 0.85, and 0.35 V on the reducing path (Fig. 2d).

The observation of more than one peak couple corresponds to previous research efforts made on nanoscaled MoS_2 [7, 18]. One possible explanation is the presence of different intercalation sites. Initially, the Li^+ ions intercalate to the layer sites in between the sheets. Afterward, the ions begin to intercalate into different defect sites as well as inter-and intra-tubular sites (in case of the tubular sample) [19]. Another possible explanation for the smaller peaks and shoulders in the CVs could be MoO_3 or other intermediate reaction products, which are like MoO_3

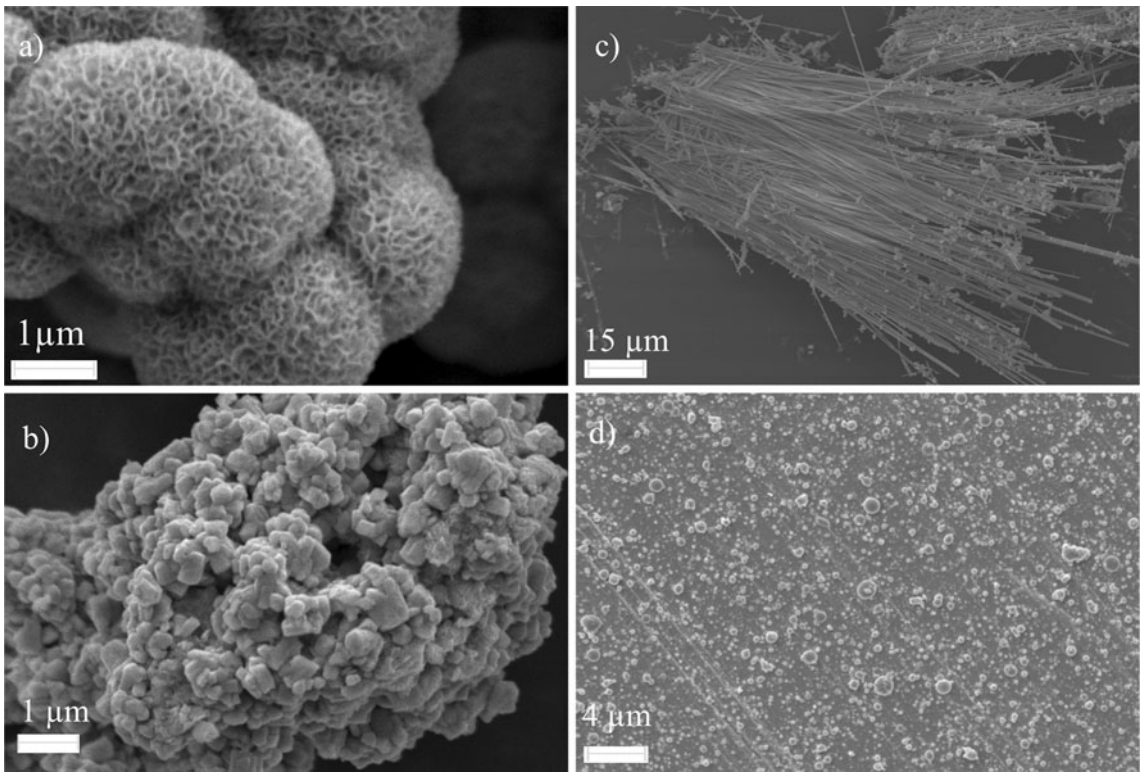

Fig. 1 SEM picture of the samples prepared via (**a**) Route (1) (**b**) Route (2) (**c**) Route (3) (**d**) PLD

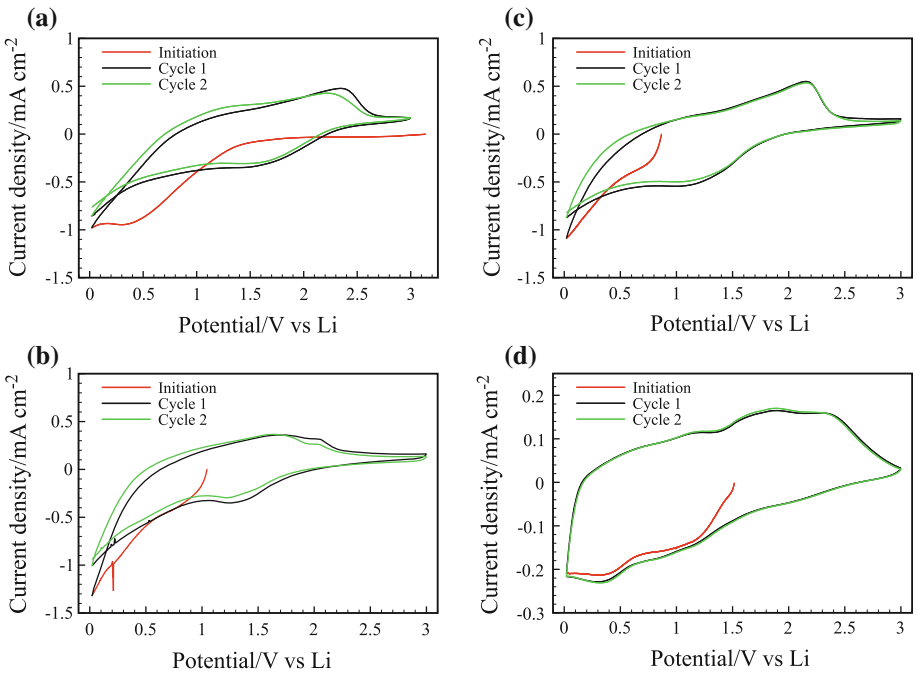

Fig. 2 CVs of samples prepared by (**a**) Route (1) (**b**) Route (2) (**c**) Route (3) (**d**) PLD

electrochemically active in Li-ion electrolytes [20]. In [2] a completely different mechanism is suggested for the potential range that was applied for the CVs. A highly reversible conversion mechanism is described where lithium and sulfur are the active materials and metallic molybdenum nanoparticles work as catalyst. But even though the lower potential barrier in our experiment is the same (0.01 V), we observe the conversion couple at 1.85 and 2.35 V [2], respectively, only for the samples prepared via Route (1) and PLD. This suggests that our materials

prepared via Route (2) and (3) in combination with the ionic liquid-based electrolyte suppress the conversion reaction $MoS_2 + 4Li^+ + 4\ e^- \rightarrow Mo + 2Li_2S$. The CVs are in general stable during the first cycles. Apart from some minor changes from the initiation to the first cycle, there are no major changes visible. The reason for the differences in the initial charging process is most likely the formation of a thin SEI at potentials of about 0.5 V [5].

The results obtained from galvanostatic cycling between 1 and 2.5 V of the nanotube, nanoflake, and thin-film electrodes are shown in Fig. 3. It is noteworthy that all samples are used in an ionic liquid-based lithium ion cell. The results reveal large differences in the gravimetric capacities and cycling stabilities. The highest capacities are achieved with the amorphous thin-film samples, showing an initial capacity of 525 mAh g^{-1}. During the following cycles, the capacity steadily increases to 528 mAh g^{-1} for the 5th cycle and 533 mAh g^{-1} for the 10th cycle, respectively. This may be attributed to an increase in surface area, due to small cracks in the film. There are no indications of a disintegration of the film, which may be attributed to the small volume changes in MoS_2. Also a conversion of the electrode is unlikely, since the potentials for the conversion reaction are below 1 V. This underlines the option to apply MoS_2 thin-films as anode in thin-film batteries. For the nanotube and the nanoflake, sample maximum capacities of 225 and 105 mAh g^{-1} are obtained. In addition, both electrode capacities rapidly fade with 20 % in the first 7 cycles for the nanotube and 8 % for the first 10 cycles in the nanoflake electrode. Figure 4 shows the cycling performance of a sample prepared via Route (1) between 1 and 2.5 V. The diagram shows a rapid capacity fade after the first three cycles. The initial capacity of 130 mAh g^{-1} decreases to about 60 mAh g^{-1} in the first 20 cycles before stabilizing around 40 mAh g^{-1} between the 30 to 50th cycle. Possible explanations for the lower capacities in the nanostructured samples could be the higher resistivity in the thicker layers (160 µm) as well as a possible loss of electrical pathways due to an insufficient amount of carbon black. Also a pulverization of the active material due to co-intercalation of the electrolyte species could cause such a breakdown. Here, further optimizations in electrode preparation, voltage control and electrolyte customization are necessary.

The diffraction pattern of the nanotubular sample shows several peaks that can be indexed to hexagonal 2H–MoS_2 [14]. The absence of the 14.4° diffraction peak in the nanotubular sample indicates the absence of stacking in the sample [21]. This suggests that the sample consists of agglomerated single sheets. Also several peaks corresponding to sulfur and molybdenum trioxide can be found. But since the CV shows no visible indications for sulfur, we conclude that the amount is very small. The sample prepared via Route (3) shows two very broad peaks around 33° and 57° with maxima that can be attributed to (011) and (−120) planes in 2H–MoS_2. The diffractogram of the nanotube powder exhibits distinct peaks, which indicates a higher degree of crystallization compared to the nanoflake powders (Fig. 5). In our case, the nanostructure with the highest degree of crystallization (Route (2), nanotubes) features a higher capacity and cycling stability compared to the less crystalline samples prepared by Route (3). This may be attributed to the special morphology of this sample since the tubular structure is able to compensate internal stress during intercalation. The diffusion coefficient might differ compared to a planar MoS_2 structure, too.

Thin-film calorimetry is used to investigate the crystallization process of a 1 µm thick MoS_2 film on top of a langasite resonator. Therefore, the resonance frequency of the coated resonator is tracked while the sample is heated. An endothermic process, such as the crystallization of amorphous MoS_2 leads to a constant temperature and resonance frequency of the resonator. The resulting curve shows a plateau of constant resonance frequency starting at 477 °C (Fig. 6). This plateau is caused by the crystallization of the film. XRD patterns before and after the heating process suggest an increasing degree of crystallization.

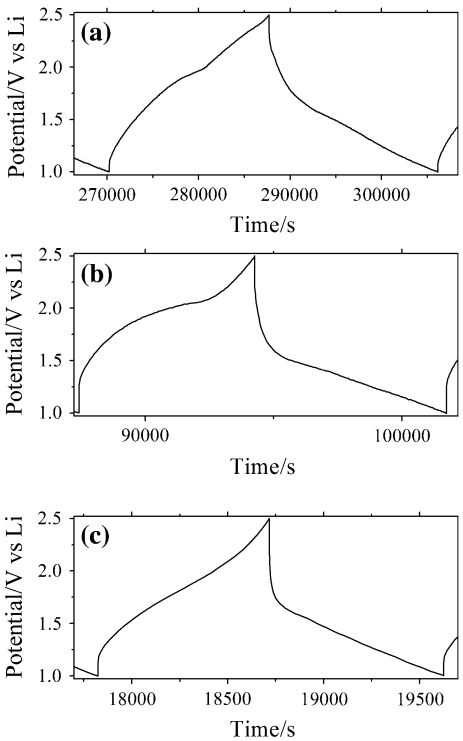

Fig. 3 Galvanostatic cycling of samples prepared by (**a**) Route (2) (**b**) Route (3) and (**c**) PLD

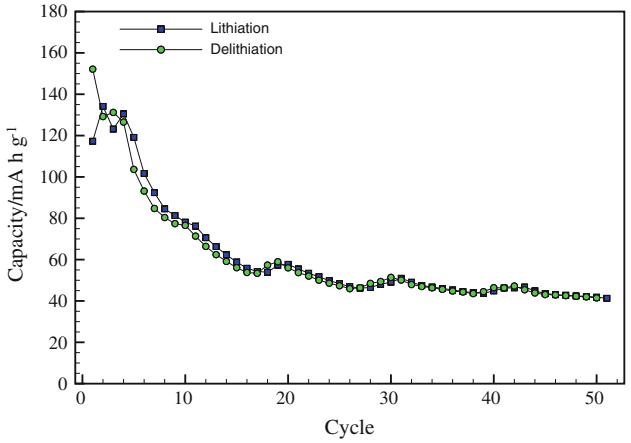

Fig. 4 Cycling performance of sample prepared via Route (1)

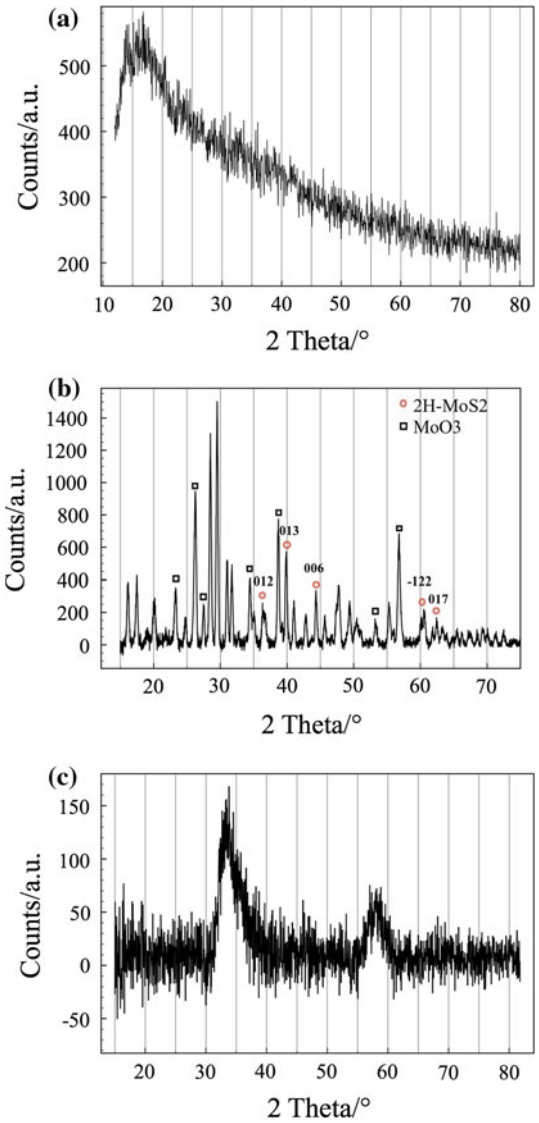

Fig. 5 Powder XRD pattern of the samples prepared by (**a**) Route (1) (**b**) Route (2) (**c**) Route (3)

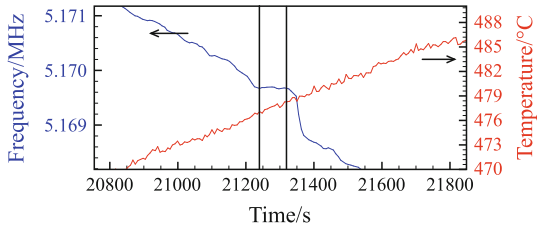

Fig. 6 Thin-film calorimetry of a MoS_2 film. The plateau with a length of about 80 s at 480 °C can be seen between the two vertical lines

4 Conclusions

Nanocrystalline and thin-film MoS_2 electrodes are prepared, operated, and electrochemically characterized in a lithium ion cell. The compatibility with Li^+TFSI^-, [BMP][TFSI] ionic liquid electrolyte is demonstrated. The prepared nanostructures show different behaviors in CV and galvanostatic cycling, respectively. The best performance is achieved with the PLD thin-film sample with 52 % of the best experimentally achieved capacity [7] and virtually no capacity loss in the first 10 cycles. The nanostructured sample's capacities are significantly smaller than the theoretically achievable capacity. Therefore, synthesis and electrode preparation should be further optimized. Even though capacity and cycling stability are not outstanding, all of the samples are in general able to work in a Li-ion secondary cell with improved safety features due to the use of the highly stable IL-based electrolyte.

Acknowledgments The authors gratefully acknowledge the financial support for this work by the German Research Foundation (DFG) as part of the priority program "Materials with New Design for Improved Lithium Ion Batteries" WeNDeLIB. We also thank M. Gensch and P. Knospe from Clausthal University of Technology for BET measurements.

References

1. Park M, Zhang X, Chung M, Less GB, Sastry AM (2010) A review of conduction phenomena in Li-ion batteries. J Power Sources 195:7904–7929
2. Fang X, Hua C, Guo X, Hu Y, Wang Z, Gao X, Wu F, Wang J, Chen L (2012) Lithium storage in commercial MoS_2 in different potential ranges. Electrochemica Acta 81:155–160
3. Sen UK, Mitra S (2013) High-rate and high-energy-density lithium-ion battery anode containing 2D MoS_2 nanowall and cellulose binder. ACS Appl Mater Interfaces 5:1240–1247
4. Xiao J, Choi D, Cosimbescu L, Koech P, Liu J, Lemmon J (2010) Exfoliated MoS_2 nanocomposite as an anode material for lithium ion batteries. Chem Mater 22:4522–4524. doi:10.1021/cm101254j
5. Guo G, Hong J, Cong C, Zhou X, Zhang K (2005) Molybdenum disulfide synthesized by hydrothermal method as anode for lithium rechargeable batteries. J Mater Sci 40:2557–2559
6. Du G, Guo Z, Wang S, Zeng R, Chen Z, Liu H (2010) Superior stability and high capacity of restacked molybdenum disulfide as

anode material for lithium ion batteries. Chem Commun 46:1106–1108. doi:10.1039/b920277c
7. Feng C, Ma J, Li H, Zeng R, Guo Z, Liu H (2009) Synthesis of molybdenum disulfide (MoS_2) for lithium ion battery applications. Mater Res Bull 44:1811–1815. doi:10.1016/j.materresbull.2009.05.018
8. Li A, Liu H, Zhu Z, Huang M, Yang Y (2006) Formation energies of the lithium intercalations in MoS_2. J Mater Sci Technol 22:40–44
9. Dominko R, Arcon D, Mrzel A, Zorko A, Cevc P, Venturini P, Gaberscek M, Remskar M, Mihailovic D (2002) Dichalcogenide nanotube electrodes for Li-ion batteries. Adv Mater 21:1531–1534
10. Miki Y, Nakazato D, Ikuta H, Uchida T, Wakihara M (1995) Amorphous MoS_2 as the cathode of lithium secondary batteries. J Power Source 54:508–510
11. Lewandowski A, Swiderska-Mocek A (2009) Ionic liquids as electrolytes for Li-ion batteries-an overview of electrochemical studies. J Power Source 194:209–601. doi:10.1016/j.jpowsour.2009.06.089
12. Aklalouch M, Amarilla JM, Rojas RM, Saadoune I, Rojo JM (2010) Sub-micrometric $LiCr_{0.2}Ni_{0.4}Mn_{1.4}O_4$ spinel as 5 V-cathode material exhibiting huge rate capability at 25 and 55°C. Electrochem Commun 12:548–552. doi:10.1016/j.elecom.2010.01.040
13. Borgel V, Markevich E, Aurbach D, Semrau G, Schmidt M (2009) On the application of ionic liquids for rechargeable Li batteries: high voltage systems. J Power Source 189:331–336. doi:10.1016/j.powsour.2008.08.099
14. Nagaraju G, Tharamani CN, Chandrappa GT, Livage J (2007) Hydrothermal synthesis of amorphous MoS2 nanofiber bundles via acidification of ammonium heptamolybdate tetrahydrate. Nanoscale Res Lett 3:461–468. doi:10.1007/s11671-007.9087-z
15. Wulfmeier H, Albrecht D, Ivanov S, Fischer J, Grieseler R, Schaaf P, Ulrich S, Bund A, Fritze H (2013) Thin-film calorimetry-device development and application to lithium ion battery materials. MRS proceedings 1496 doi:10.1557/opl.2013.104
16. Fritze H (2011) High-temperature bulk acoustic wave sensors. Meas Sci Technol 22:12002. doi:10.1088/0957-0233/22/1/012002
17. Ashfold M, Claeyssens F, Fuge G, Henley S (2003) Pulsed laser deposition of thin-films. Chem Soc Rev 33:23–31. doi:10.1039/B207644F
18. Li H, Li W, Ma L, Chen W, Wang J (2009) Electrochemical lithiation/delithiation performances of 3D flowerlike MoS_2 powders prepared by ionic liquid assisted hydrothermal route. J Alloy Compd 471:442–447. doi:10.1016/j.jallcom.2008.03.133
19. Wang GX, Bewlay S, Yao J, Liu HK, Dou SX (2004) Tungsten disulfide nanotubes for lithium storage. Electrochem Solid State Lett 7:A321–A323. doi:10.1149/1.1788591
20. Swiatowska-Mrowiecka J, de Diesbach S, Maurice V, Zanna S, Klein L, Briand E, Vickridge I, Marcus P (2008) Li-ion intercalation in thermal oxide thin-films of MoO_3 as studied by XPS, RBS and NRA. J Phys Chem 112:1105011058
21. Peng Y, Meng Z, Zhong C, Lu J, Yu W, Yang Z, Qian Y (2001) Hydrothermal synthesis of MoS_2 and Its pressure-related crystallization. J Solid State Chem 159:170–173. doi:10.1006/jssc.2001.9146